Long survival of PD-L1-positive mediastinal sarcomatoid carcinoma after immunotherapy and anti-angiogenic target therapy: A case report

SHULING WU[1*], DANPING WANG[1*], QIONG FU[2] and YINGYING DING[1]

[1]Department of Respiratory and Critical Care Medicine, The First People's Hospital of Xiaoshan District, Hangzhou, Zhejiang 311200, P.R. China; [2]Department of Pathology, The First People's Hospital of Xiaoshan District, Hangzhou, Zhejiang 311200, P.R. China

Received December 5, 2025; Accepted June 3, 2026

DOI: 10.3892/ol.2026.15690

Abstract. Mediastinal sarcomatoid carcinoma (SC) is rare and is often associated with poor survival outcomes. At present, there have been no investigations into the use of immunotherapy and anti-angiogenic target therapy to treat mediastinal SC. In the present study, a 74-year-old woman with mediastinal SC who achieved long-term survival was described. Immunohistochemistry of tumor specimens showed high expression of programmed cell death ligand 1 (PD-L1) and a combined positive score of 80. The patient initially received two cycles of chemotherapy and one cycle of radiotherapy combined with anlotinib; subsequent evaluation confirmed stable disease. After which, the patient received two cycles of immunotherapy with durvalumab, and received continued administration with anlotinib; follow-up evaluation revealed a partial response. Immunotherapy was halted due to severe adverse effects, but treatment with anlotinib has remained ongoing. At present, the patient remains alive with no evidence of disease progression, achieving a progression-free survival of >42 months. The present case report highlights the potential of immunotherapy combined with anti-angiogenic targeted therapy in treating PD-L1-positive mediastinal SC, despite the life-threatening adverse reactions, offering a viable treatment option for similar clinical cases.

Correspondence to: Dr Yingying Ding, Department of Respiratory and Critical Care Medicine, The First People's Hospital of Xiaoshan District, 199 Shixin South Road, Xiaoshan, Hangzhou, Zhejiang 311200, P.R. China
E-mail: 18967100837@163.com

*Contributed equally

Key words: mediastinal sarcomatoid carcinoma, immunotherapy, immune checkpoint inhibitor, anti-angiogenic target therapy, anlotinib

Introduction

Sarcomatoid carcinoma (SC) is a rare type of biphasic cancer characterized by the presence of both epithelial and mesenchymal tumor cells. According to Xu *et al* (1) the age-adjusted incidence of SC was 1.26/100,000 individuals in 2014, and the average onset age of SC is 68±13 years (1). The prevalence of SC is highest in the respiratory system, followed by digestive, urinary and female genital systems (1). SC of the lungs, urinary bladder and liver is reported to predominantly affect male patients (2-4). Mediastinal SC is an aggressive malignancy with limited documentation in existing literature. It may originate from the thymus or pulmonary tissue. Patients often present with non-specific symptoms such as cough, chest pain and breathlessness (5-10). Due to the invasiveness and frequent metastasis, SC is often diagnosed at an advanced stage (2). Patients with early-stage SC can benefit from surgical intervention. For advanced stage SC, the therapeutic efficacy of chemotherapy and radiotherapy remains modest (2-4). Due to its high malignancy, late detection and poor response to conventional chemoradiotherapy, the prognosis for SC is generally unfavorable (2). In the present case report, a patient with mediastinal SC who achieved prolonged progression-free survival (PFS) after treatment is described. This case is notable not only because of the uncommon anatomical location but also due to the favorable clinical outcome challenging the established perception of universally poor prognosis in this malignancy. Through detailed presentation and comprehensive review of clinical features, pathological features and treatment, the present case report aims to expand the extremely limited evidence base for this rare disease entity and identify potential therapeutic strategies, addressing the key knowledge gap regarding optimal management of mediastinal SC.

Case report

Case presentation. A 74-year-old female patient with no history of smoking presented to The First People's Hospital of Xiaoshan (Hangzhou, China) in January 2022 with cough and chest pain for 50 days, and breathlessness and dysphagia for 10 days. Physical examination revealed a mobile 3 cm

lymph node in the right neck, and audible wheezing sounds from both lungs. The patient had a history of hypertension and diabetes for >20 years, but blood pressure and blood glucose levels were well-controlled with medication. In addition, the patient reported no family history of cancer. A chest computed tomography (CT) scan was performed, which revealed a mass with soft tissue density and spotted calcification at the right posterior upper mediastinum (maximum cross-section, 8.5x6.2 cm). Furthermore, the trachea and esophagus were compressed and deformed. Finally, a contrast-enhanced chest CT scan was performed the following day, which showed inhomogeneous enhancement contrast (Fig. 1).

A total of 4 days after the patient presented to the hospital, a bronchoscopy examination was performed, which revealed notable stenosis in the middle and lower segments of the trachea due to external pressure. In addition, an endobronchial ultrasound showed abnormal low-density echogenicity on the right posterior side of the trachea. Transbronchial needle aspiration was performed and a tracheal stent of 16x40 mm was placed, which notably alleviated bronchial stenosis. H&E staining of the specimen showed multiple small clusters of atypical cells scattered in the background of mucus and inflammatory cells, with an abundant cytoplasm and lack of specificity in immunohistochemical markers. Fluorodeoxyglucose positron emission tomography (FDG PET) was performed the following day at Zhejiang Aibo Medical Imaging Diagnosis Center (Hangzhou, China), which showed a soft tissue density mass with increased FDG uptake in the posterior mediastinum with unclear margins relative to the bronchus, carina and right main bronchus, suggesting a high probability of mediastinal-type lung cancer. FDG PET also showed multiple enlarged lymph nodes in the right supraclavicular, cervical, mediastinal 2R and 4R lymph nodes with a mild increase in FDG metabolism. These findings suggested reactive lymph node hyperplasia, with a very low possibility of lymph node metastasis to be excluded. A fine-needle aspiration biopsy of the lymph node in the right cervical was conducted and the pathological results indicated chronic inflammation of the lymph nodes.

Only a small portion of the specimen consisted of tumor cells, and it lacked specificity in immunohistochemical markers, thus a clear pathological diagnosis was not achieved. The patient was sent to The First Affiliated Hospital of Medical School of Zhejiang University (Hangzhou, China) at the end of January 2022 for further treatment. The patient underwent gastroscopy and endoscopic ultrasound-guided fine needle aspiration (EUS-FNA). After tissue was fixed with 4% formalin, 4-μm paraffin sections were prepared and processed according to standard procedures. The staining steps included hematoxylin nuclear staining at room temperature (RT) for 5-10 min, followed by eosin cytoplasmic staining at RT for 2-3 min. Microscopically, H&E staining (Fig. 2) revealed sarcoma-like neoplasms. Immunohistochemical (IHC) analysis demonstrated positivity for epithelial membrane antigen (EMA) (Fig. 3A), transducing-like enhancer of split 1 (TLE1) (Fig. 3B) and smooth muscle actin (SMA), along with other immunological markers including histone h3 lysine 27 trimethylation (H3K27Me3), mouse double minute 2 homolog (MDM2), caldesmon and epithelial cadherin (E-Cad). By contrast, the sample was negative for several markers including cytokeratin (CK) (Fig. 3C), cluster of differentiation 117 (CD117), S-100 protein (S-100), desmin (Des), CD34, human melanoma black 45 antigen (HMB45), anaplastic lymphoma kinase (ALK), SRY-box transcription factor 10 (SOX-10), signal transducer and activator of transcription 6 (STAT6), tumor protein p63 (P63), CK5/6, CD68, myogenic differentiation 1 (MyoD1), CD30, spalt-like transcription factor 4 (SALL4), CK7, CD10, estrogen receptor (ER), discovered on gist 1 (DOG-1) and cyclin-dependent kinase inhibitor 2a (P16). Additionally, high expression of proliferation index (Ki-67) (70% positive; Fig. 3D) was noted. IHC protocol summary: The samples were fixed in 10% neutral buffered formalin for 24-48 h at RT, embedded in paraffin and sectioned at a thickness of 3-5 μm. After epitope retrieval (EDTA repair solution, 100˚C, 20 min), samples were blocked with endogenous peroxidase blocker included in the DAB Detection Kit (ready-to-use)

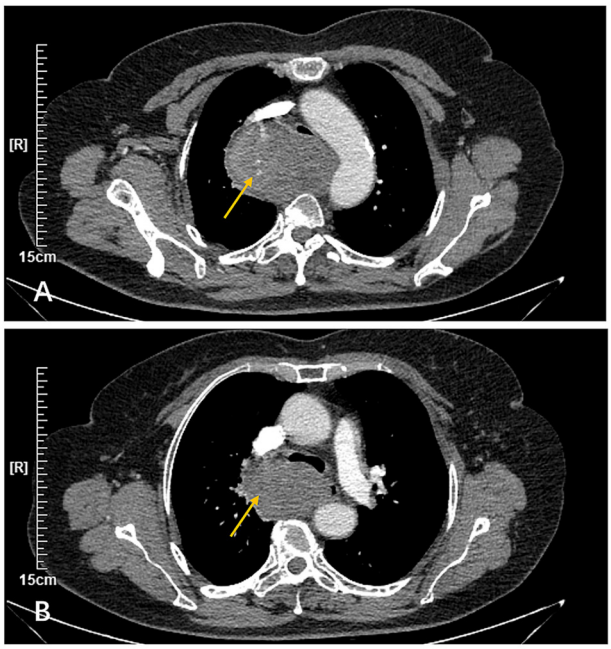

Figure 1. Baseline contrast-enhanced chest computed tomography in January 2022. (A) Maximum cross-sectional area showing a soft tissue mass measuring 8.5x6.2 cm (yellow arrow) at the right posterior upper mediastinum with uneven density and spotted calcification, and a compressed and deformed trachea and esophagus. Inhomogeneous enhancement was observed after injecting iodinated contrast medium. (B) Subcarinal cross-sectional area showing a soft tissue mass measuring 6.6x4.4 cm (yellow arrow).

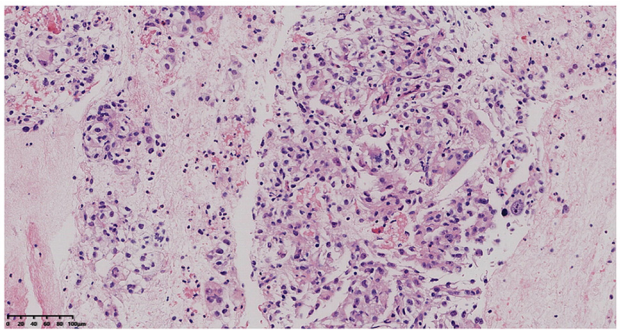

Figure 2. Pathology of the specimen obtained through endoscopic ultrasound-guided fine needle aspiration showing sarcoma-like tumors. (H&E staining; magnification, x200; scale bar, 100 μm).

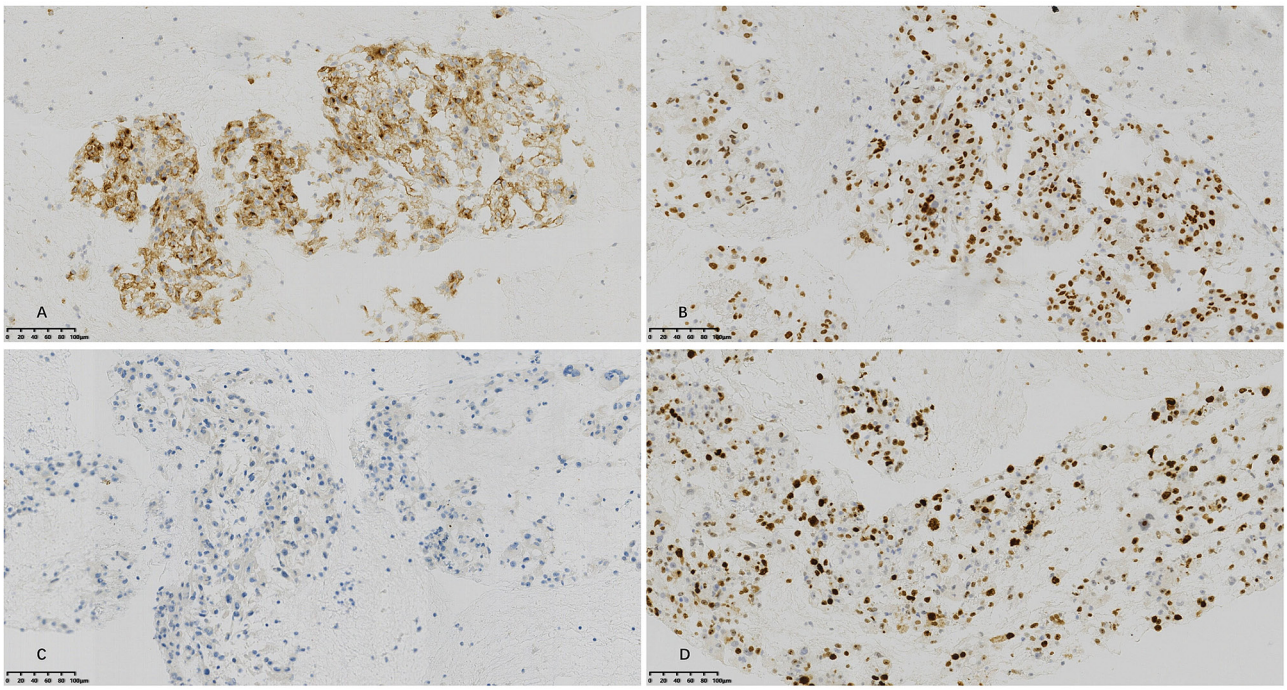

Figure 3. Representative immunohistochemical images demonstrating: (A) EMA (+, yellow or brown-yellow); (B) TLE1 (+, yellow or brown-yellow); (C) CK (-); and (D) Ki-67 (~70% nuclear positivity, yellow or brown-yellow) (magnification, x200; scale bar, 100 μm).

for 10 min at RT. They were then incubated with primary antibodies at RT for 40 min and then with secondary antibody (sheep anti-rat/rabbit IgG polymer horseradish peroxidase; cat. no. PV8000D; ready-to-use; Beijing Zhongshan Jinqiao Biotechnology Co., Ltd.) at RT for 15 min. Primary antibodies against EMA (cat. no. Kit-0011; ready-to-use), CD117 (cat. no. Kit-0029; ready-to-use), CD34 (cat. no. Kit-0004; ready-to-use), MyoD1 (cat. no. MAB-0822; ready-to-use), CD30 (cat. no. MAB-0023; ready-to-use), SALL4 (cat. no. MAB-0691; ready-to-use), CD10 (cat. no. MAB-0668; ready-to-use), P16 (cat. no. MAB-0673; ready-to-use) and Des (cat. no. MAB-0766; 1:100 dilution) were from Fuzhou Maixin Biotechnology Development Co., Ltd. Primary antibodies against MDM2 (cat. no. ZM-0425; ready-to-use), Cladesmon (cat. no. ZA-0535; ready-to-use), E-Cad (cat. no. ZA-0565; ready-to-use), S-100 (cat. no. ZM-0224; ready-to-use), HMB45 (cat. no. ZM-0187; ready-to-use), ALK (cat. no. ZM-0848; ready-to-use), SOX-10 (cat. no. ZA-0624; ready-to-use), STAT6 (cat. no. ZA-0647; ready-to-use), CK5/6 (cat. no. ZM-0313; ready-to-use), CD68 (cat. no. ZM-0060; ready-to-use), CK (cat. no. ZM-0069; 1:200), P63 (cat. no. ZM-0406; 1:200), CK7 (cat. no. ZM-0071; 1:100), Ki-67 (cat. no. ZM-0166; 1:200) and SMA (cat. no. ZM-003; 1:100) were from Beijing Zhongshan Jinqiao Biotechnology Co., Ltd. Primary antibodies against TLE1 (cat. no. ab183742; 1:250), H3K27Me3 (cat. no. ab6002; 1:1,000) and ER (cat. no. ab16660; 1:200) were from Abcam plc. Primary antibody against DOG-1 (cat. no. 54598S; 1:200) was from Cell Signaling Technology, Inc. Diaminobenzidine was used to visualize the staining and then the slides were counterstained with hematoxylin, followed by observation with a light microscope. Fluorescence *in situ* hybridization (FISH) analysis revealed no significant amplification of MDM2/centromere 12 (CEP12). FISH protocol summary: Tissue samples were fixed in 10% neutral buffered formalin for 12-24 h and routinely processed into paraffin blocks. Formalin-fixed paraffin-embedded (FFPE) tissue sections (4 μm) were baked at 70˚C for 10 min, deparaffinized in xylene (10 min, 2 times) and rehydrated through a graded ethanol series (100, 100, 90, and 70%; 5 min each). Heat pretreatment was performed using the Vysis Paraffin Pretreatment Reagent Kit (Abbott Molecular, Inc.). Briefly, slides were immersed in pretreatment solution at 80˚C for 25-30 min, rinsed in distilled water (2 min, 2 times) and digested with Protease IV at 37˚C for 15 min. After a 3-min wash in distilled water, sections were dehydrated in ethanol (70, 85 and 100%; 1 min each) and air-dried. The Vysis LSI MDM2/CEP12 FISH Probe Kit (cat. no. 01N15-010; Abbott Molecular Inc.) was then applied according to the manufacturer's instructions. Briefly, 10 μl of probe mixture was pipetted onto each specimen, covered with a 22x22 mm coverslip and sealed with rubber cement. Probe and target DNA were co-denatured on a HYBrite denaturation/hybridization system at 72˚C for 5 min and hybridized overnight (16-24 h) at 37˚C in a humidified chamber. Post-hybridization washes were conducted in prewarmed 0.4X saline-sodium citrate containing 0.3% Nonidet P-40 at 73˚C for 2 min, followed by dehydration in ethanol (70, 85 and 100%; 1 min each). Slides were counterstained with DAPI II antifade solution (Abbott Molecular) and examined under a fluorescence microscope equipped with single-bandpass filters for DAPI (excitation 358-405 nm), Spectrum Green (excitation ~495 nm) and Spectrum Orange (excitation ~546 nm), using a x100 oil-immersion objective. Signal enumeration and MDM2/CEP12 ratio calculations were performed using GenASIs software. A case was considered MDM2-amplified when the MDM2/CEP12 signal ratio was ≥2.0 in at least 50 evaluable tumor nuclei. The EUS-FNA specimen was sent to

Shanghai Fudan University Affiliated Zhongshan Hospital (Shanghai, China), where the SYT gene mutation was tested using FISH; the result was negative. The EMA-positive results combined with the morphological features suggested a diagnosis of SC or synovial sarcoma. However, the absence of SYT gene mutation ruled out the possibility of synovial sarcoma. Therefore, the patient was diagnosed with EMA-positive SC [specifically mediastinal SC (cT4N0M0, IIIA)] in February 2022. Although pathological findings alone were inconclusive for determining tumor origin, when considered in conjunction with radiological features, a pulmonary origin was regarded as the most likely diagnosis.

The specimen obtained via bronchoscopy was sent to Amoy Diagnostics Co., Ltd. for genomic and programmed cell death ligand 1 (PD-L1) testing; no pathogenic gene mutations were detected. PD-L1 expression was evaluated using Leica Bond-Max (Leica Biosystems), with antibody clone E1L3N. The samples were prepared into FFPE tissue section, with a thickness of 3-5 μm. After epitope retrieval (Bond epitope retrieval ER2 solution, 100˚C, 20 min), samples were blocked with peroxide block (included in the Leica BOND Polymer Refine Detection kit; cat. no. DS9800; ready-to-use; Leica Biosystems) at RT for 5 min. They were then incubated with primary antibody (PD-L1 antibody; cat. no. 13684; ready-to-use; Cell Signaling Technology, Inc.) at RT for 10 min and then with secondary antibody (polymer; cat. no. DS9800; ready-to-use; Leica Biosystems) at RT for 12 min. Diaminobenzidine was used to visualize the staining and then the slides were counterstained with hematoxylin, followed by observation with a light microscope. Positive, negative and blank controls were included in each staining run. The Positive control consisted of one weakly positive and one strongly positive PD-L1-expressing non-small cell lung cancer (NSCLC) formalin-fixed paraffin-embedded tissue section. CPS was calculated as the ratio of viable tumor cells and tumor-associated immune cells (lymphocytes and macrophages) with any staining intensity to the total viable invasive tumor cells, multiplied by 100. Pathologists determined the final results via light microscopy. Firstly, the entire tissue section was scanned at 10x magnification to ensure ≥100 viable tumor cells for sample adequacy; then staining tumor cells and tumor-associated immune cells were counted at 20x magnification (confirmation at 40x magnification if needed) and applied to the formula. Immunohistochemistry revealed high expression of PD-L1, with a combined positive score (CPS) of 80 (Fig. 4).

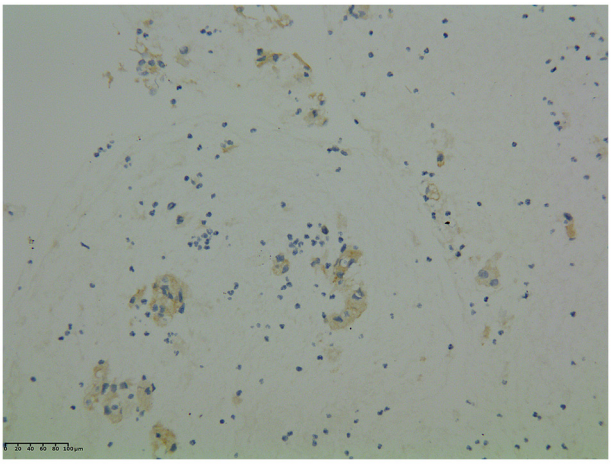

Figure 4. Representative PD-L1 immunohistochemical images showing high expression (CPS=80). The brown DAB staining indicates PD-L1 expression on the cell membrane, while blue hematoxylin counterstain marks the nuclei (magnification, x200; scale bar, 100 μm).

Treatment process. The patient received multiple treatment protocols consecutively. Initial first-line treatment, which commenced in February 2022, consisted of chemotherapy (cisplatin and albumin-bound paclitaxel) and antiangiogenic targeted therapy (anlotinib; 12 mg once daily). Due to severe gastrointestinal adverse reactions, the second chemotherapy regimen was changed to carboplatin and albumin-bound paclitaxel in March 2022. Concurrent radiotherapy (4,000 cGy/20F to 95% PTV) was initiated in March 2022, while anlotinib was maintained. After the second chemotherapy cycle, treatment was discontinued due to a grade-3 myelosuppression. A chest CT in March 2022 revealed a mass measuring 8.3x6.2 cm at the maximum cross-section (Fig. 5B), which was slightly decreased in size compared with the initial measurement taken in January 2022 (Fig. 5A). The overall treatment response was evaluated as stable disease (SD).

The patient received two cycles of immunotherapy (durvalumab; 1,000 mg) in April 2022 and May 2022, whilst continuing treatment with anlotinib (10 mg once daily). A total of 7 days after the second immunotherapy cycle, the patient developed limb weakness, pain in the proximal limbs and chest pain, and was subsequently hospitalized again in May 2022. In May 2022, laboratory results demonstrated elevated levels of biomarkers, including aspartate aminotransferase at 488 U/l (upper limit, 35 U/l), alanine aminotransferase at 209 U/l (upper limit, 40 U/l), creatine kinase at 7,933 U/l (upper limit, 35 U/l), creatine kinase isoenzyme MB at 142.65 μg/l (upper limit, 5 μg/l) and troponin T at 0.585 μg/l (upper limit, 0.014 μg/l). Results from an electrocardiogram performed in May 2022 were normal. However, when retested 8 days later in June 2022, ST-segment abnormalities and frequent premature atrial beats were recorded (Fig. 6). Transthoracic echocardiography in May 2022 demonstrated mild regurgitation of the aortic, mitral and tricuspid valves. Single photon emission computed tomography (SPECT) myocardial perfusion imaging performed in June 2022 revealed no significant perfusion defects in the left ventricular myocardium and normal left ventricular systolic function.

During the exacerbation of symptoms, the patient exhibited no fever or other infectious manifestations. Laboratory results demonstrated normal leukocyte counts at $6.73x10^9$/l (reference range,$3.50\text{-}9.50x10^9$/l), normal neutrophil counts at $5.18x10^9$/l (reference range, $1.8\text{-}6.3x10^9$/l) and mildly elevated CRP at 26 mg/l (upper limit, 8 mg/l). The magnitude of CRP elevation was substantially disproportionate to the degree of clinical worsening observed, thereby rendering an infectious etiology unlikely. Serological tests demonstrated mildly elevated serum IgG levels at 26.1 g/l (upper limit, 16 g/l), whereas antinuclear antibodies profiles, antineutrophil cytoplasmic antibodies profiles, rheumatoid factor, anti-cyclic citrullinated peptide, immunoglobulins (IgA, IgM) and complements (C3, C4) were all negative; hence, autoimmune diseases were

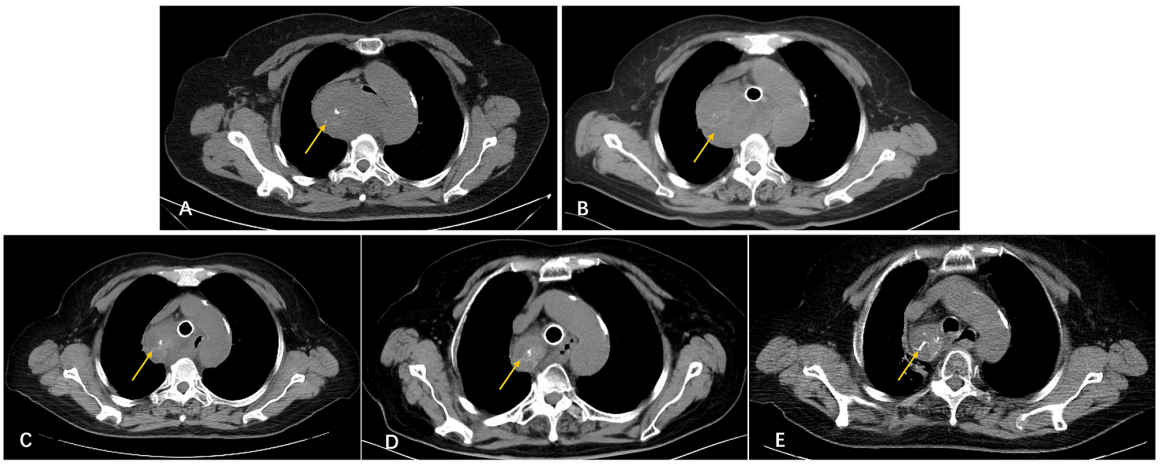

Figure 5. Chest computed tomography before and after treatment. (A) Soft tissue mass measuring 8.5x6.2 cm (yellow arrow) at the maximum cross-sectional area in January 2022. (B) Soft tissue mass measuring 8.3x6.2 cm (yellow arrow) at the maximum cross-sectional area in March 2022. (C) Soft tissue mass measuring 5.5x4.8 cm (yellow arrow) at the maximum cross-sectional area in May 2022. (D) Soft tissue mass measuring 3.5x2.4 cm (yellow arrow) at the maximum cross-sectional area in July 2022. (E) Soft tissue mass measuring 3.5x2.4 cm (yellow arrow) at the maximum cross-sectional area in July 2025.

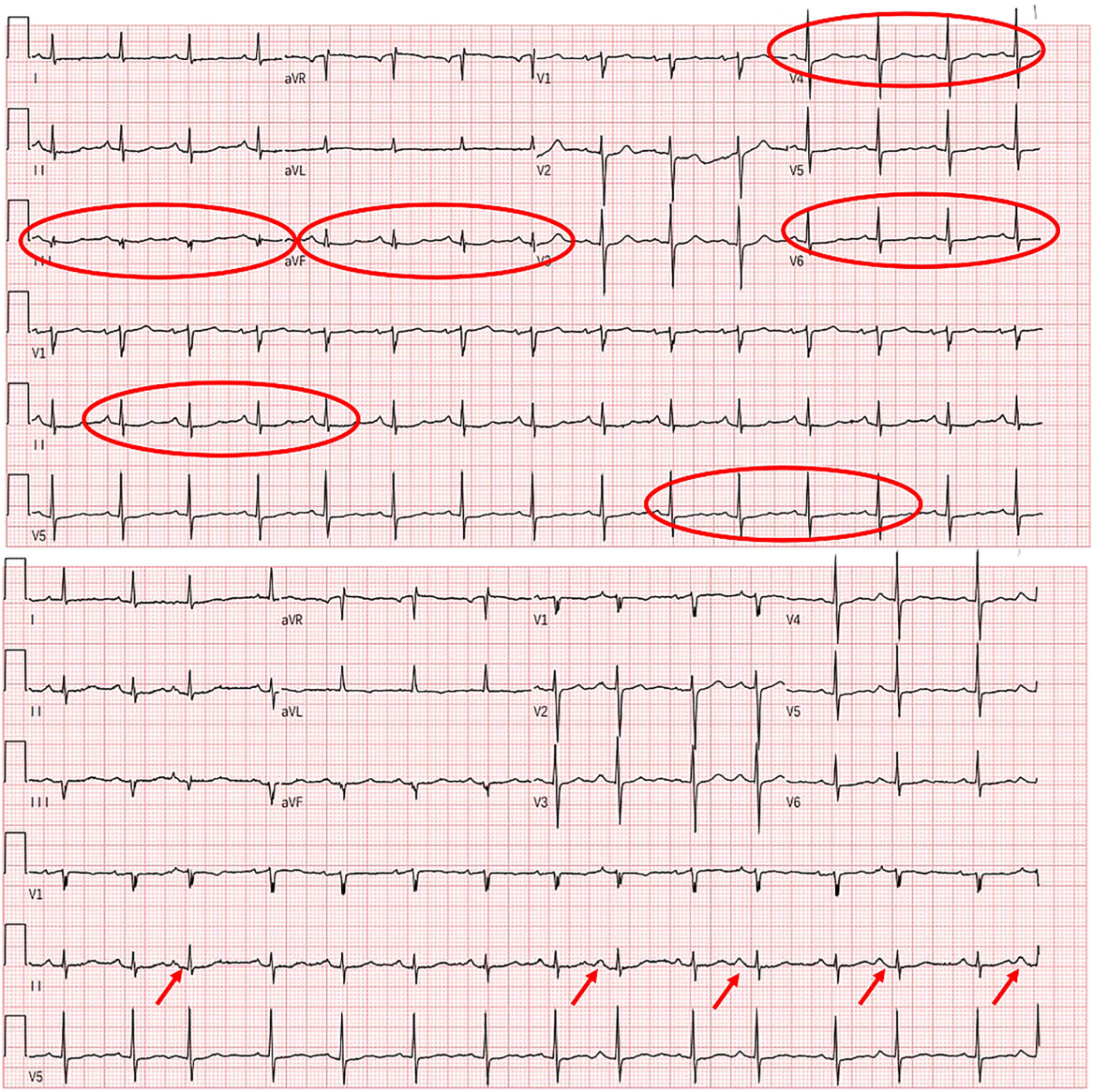

Figure 6. ECG images after immunotherapy showed ST-segment changes (in leads II, III, aVF, V4, V5 and V6, red circles) and premature atrial contractions (red arrows).

Table I. Timeline of the case.

Date	February 2022	February-March 2022	March 2022	April-May 2022	May 2022-July 2025
Event	Diagnosis	Chemotherapy, anlotinib	Radiotherapy, anlotinib	Immunotherapy, anlotinib	anlotinib
Response	N/A	SD	SD	PR	PR
Toxicities	N/A	Gastrointestinal adverse reactions and grade-3 myelosuppression	Not observed	Grade-3 immune-related myocarditis, myositis and hepatitis	Not observed

SD, stable disease; PR, partial response.

excluded. Following exclusion of infection and autoimmune diseases, and given the lack of exposure to other potentially causative medications, the patient was diagnosed with grade-3 immune-related myocarditis, grade-3 immune-related myositis and grade-3 immune-related hepatitis.

In May 2022, the patient started receiving high-dose methylprednisolone (80 mg every 12 h). Additionally, intravenous immunoglobulin pulse therapy (20 g/day) was administered for 3 days. The detailed methylprednisolone tapering regimen was as follows: The patient received intravenous methylprednisolone 80 mg every 12 h for 4 days, 40 mg every 8 h for 4 days, 40 mg every 12 h for 6 days and 30 mg every 12 h for 6 days. The route was subsequently switched to oral administration at 40 mg once daily for 7 days, and further reduced to 32 mg once daily, followed by gradual dose reduction for long-term maintenance. The patient gradually recovered from the severe condition and was discharged in June 2022. Due to the severe immune-related myocarditis, myositis and hepatitis, immunotherapy was halted and long-term anti-angiogenic targeted therapy with anlotinib (10 mg once daily) was maintained, with the last prescription date in September 2025.

Treatment outcomes and follow-up. After two cycles of immunotherapy combined with anti-angiogenic targeted therapy, the patient underwent multiple follow-up chest CT scans. A chest CT in May 2022 (Fig. 5C) and July 2022 (Fig. 5D) indicated that the mediastinal mass continued to shrink. In May 2022, the soft tissue mass was 5.5x4.8 cm at the maximum cross-sectional area. By July 2022, the soft tissue mass had decreased to 3.5x2.4 cm, confirming a clinical evaluation of partial response (PR). Subsequent follow-up chest CT showed that the mediastinal mass remained stable until July 2025 (last chest CT date; Fig. 5E). FDG PET was performed again in May 2024 and showed a soft tissue mass in the right upper mediastinum with mildly increased FDG uptake, suggesting tumor activity after therapy. At present (as of July 2025), the patient is alive and the PFS is >42 months. The diagnostic procedures, therapeutic procedures and tumor responses are all summarized in Table I.

Discussion

SC is a rare and aggressive subtype of cancer (1). It is characterized by the presence of both epithelial and mesenchymal components, with the mesenchymal components considered epithelial in origin (2). The epithelial components typically possess varying degrees of CK and EMA expression, while the sarcomatoid components commonly express vimentin (2). Previous studies have shown an increased Ki67 index in SC, which is associated with a worse prognosis (11,12). In addition, a lack of CK expression does not rule out the diagnosis of SC (12). In the present case report, microscopy revealed the presence of scattered spindle and polygonal cells, indicating mesenchymal differentiation. Immunohistochemical analysis demonstrated positivity for EMA, confirming epithelial origin, while high expression of Ki67 (70%) confirmed the aggressiveness of tumor cell proliferation.

SC can occur in various systems and organs, but is mainly in the respiratory system (1). The occurrence of SC in the mediastinum is particularly rare. It typically originates from the thymus or pulmonary tissue. Several case reports have previously documented mediastinal thymic SC (5-9). However, to the best of our knowledge, there has been only one published case report describing a patient with mediastinal pulmonary SC (PSC) (10).

Differential diagnosis between thymic SC and PSC remains challenging given their morphologic overlap, yet they carry key therapeutic implications. As summarized in Table II, these two entities diverge markedly in anatomic distribution, immunophenotype, molecular profiles and treatment outcomes (13-16). Specifically, thymic SC typically localizes to the anterior mediastinum with possible CD5/CD117 positivity and lacks well-defined driver mutations (13,14), whereas PSC arises from pulmonary parenchyma, bronchus or posterior mediastinum, shows MET/KRAS/EGFR/TP53/ALK alterations and exhibits distinct immunohistochemistry patterns (15,16).

In the present case, the absence of p63, CK5/6 and CK7 expression argues against a conventional pulmonary squamous cell carcinoma origin, while the absence of TTF-1 and Napsin A staining data precludes definitive determination of a pulmonary adenocarcinoma origin. Additionally, the positive EMA staining confirms the epithelial derivation of this neoplasm. Due to exhaustion of available tissue specimens, additional immunohistochemical staining for TTF-1 and Napsin A could not be performed. However, SC frequently undergo extensive epithelial-mesenchymal transition, resulting in diminished or complete loss of conventional lung-lineage markers, including TTF-1, Napsin A, p63 and CK5/6 (17). Therefore, the absence

Table II. Comparison between pulmonary SC and thymic SC.

Diseases	Pulmonary SC	Thymic SC	(Refs.)
Incidence	0.3-3% of all pulmonary types of cancer	~4% of thymic types of cancer	(13,15)
Location	Lung; trachea and bronchus; posterior mediastinum, involving trachea/bronchus	Anterior mediastinum	(14,15)
IHC markers	CKs$^+$; EMA$^+$; vimentin$^+$; TTF-1$^+$ and Napsin A$^+$ in case of adenocarcinoma origin; p40$^+$ and high-molecular-weight CKs$^+$ in case of squamous cell carcinoma origin	CK$^+$; vimentin$^+$; CK5/6$^+$; CK7$^+$; p63/p40$^+$; PAX8$^+$; CD5$^{+/-}$; CD117$^{+/-}$	(14,15)
Molecular landscape	MET exon 14 skipping mutation; KRAS (mostly G12C) mutation; EGFR mutation; TP53 mutation; ALK mutation;	Not reported	(14,15)
Treatments	Surgery; molecular targeted therapy; immunotherapy; chemotherapy; radiotherapy	Surgery; standard chemotherapy/ radiotherapy, subtype-specific data lacking	(14-16)
Prognosis	Median OS: 6.3 months in the chemotherapy era; 22.8 months in the immunotherapy era (small-scale retrospective study);	OS: 2 months to 3 years [no statistical data, only case reports]	(5-9,16)

IHC, immunohistochemical; SC, sarcomatoid carcinoma.

of these immunohistochemical markers does not necessarily exclude a pulmonary origin. The pathological findings, in conjunction with radiological examination, support a clinical diagnosis of PSC in the present case report.

The prognosis for SC is generally unfavorable (2). Specifically, patients with PSC have a median overall survival (OS) of ~6.3 months (3). For individuals with mediastinal thymic SC, the OS ranges from 2 months to 3 years (6-9). However, due to the rarity of thymic SC, comprehensive statistical data regarding OS remains unavailable. Although, with the emergence of novel treatment methods, the therapeutic effects and survival time for PSC have improved notably.

Similar to other types of cancer, patients with early-stage SC can benefit from surgical intervention. Patients with SC of the lungs or liver who receive surgical treatment generally have longer OS than those who do not (18,19). A case report describing a case of mediastinal thymic SC reported that the patient had an OS of 13 months after receiving surgery as the only treatment (6).

For advanced stage SC, the therapeutic efficacy of chemotherapy remains modest. According to Vieira *et al* (20), the median PFS of patients with PSC receiving first-line chemotherapy was 2.0 months, and the median OS was 6.3 months (20). This was markedly shorter than other NSCLC subtypes (median PFS, 4.3 months; median OS, 8.9 months) (21). Similarly, chemotherapy regimens that are effective for other intestinal malignancies have demonstrated limited efficacy in patients with small-intestinal SC (22). This is demonstrated by a case report describing a patient with thymic SC who experienced progressive disease after two cycles of chemotherapy with paclitaxel and carboplatin (8).

Studies on the effect of radiotherapy in SC have different outcomes. For example, in a retrospective study, patients with PSC who received adjuvant radiotherapy had a 5-year survival rate of 55.4%, while those who did not had a 5-year survival rate of 29.4% ($P<0.01$) (23). However, Rahouma *et al* (24) reported a decreased OS for patients with PSC who received radiotherapy. Furthermore, a study by Zhu *et al* (22) concluded that radiotherapy is ineffective for small intestine SC. Although, one case report described a patient with thymic SC that had an OS of 28 months after chemotherapy and radiotherapy, indicating the possible effectiveness of radiotherapy in thymic SC (8).

In the present case report, after two cycles of chemotherapy and one cycle of radiotherapy, the efficacy evaluation was considered SD. This indicated the limited effectiveness of chemotherapy and radiotherapy in mediastinal SC, but further studies are needed to confirm this.

Immune checkpoint inhibitors (ICIs) monotherapy or combination therapy have shown good efficacy in NSCLC and other types of epithelial cancer (25). Multiple studies have shown that ICIs achieve substantially improved outcomes in patients with advanced NSCLC with high PD-L1 expression (tumor proportion score, ≥50%) compared with conventional chemotherapy (25-27). At present, PD-L1 is an FDA-approved biomarker for predicting the efficacy of ICIs in patients with pulmonary cancer (25). PD-L1 has high expression in PSC, with expression in the sarcomatoid component higher than in the epithelial component (28). A retrospective study showed that 83% of cases with pancreatic SC had a CPS ≥1 and 50% of the cases had a CPS ≥50 (29).

There are several retrospective studies investigating the efficacy of ICIs in SC. In a study by Roesel *et al* (30), patients with PSC had favorable responses to ICIs after first-line and second-line chemotherapy failed to show positive results. Qian *et al* (31) reported a median PFS of 9.2 months and median OS of 22.8 months in a cohort of 21 patients with PSC that received first-line immunotherapy (31), notably surpassing

the 2.0-month PFS and 6.3-month OS previously observed with chemotherapy alone (20). Notably, there are no statistical differences in PFS or OS among different ICIs (31). In a retrospective study, PD-L1-positive patients with PSC have longer median PFS than PD-L1-negative patients (17.50 months vs. 6.07 months; P=0.812) (32). Wang *et al* (33) also observed that ICIs demonstrate enhanced efficacy in patients with SC of the head and neck that have higher PD-L1 expression. These two studies indicate that PD-L1 may be a useful biomarker for predicting the effect of ICIs in advanced SC. However, more prospective studies are required to confirm this.

Angiogenesis is essential for the growth and metastasis of carcinomas; consequently, anti-angiogenic targeted therapy has been widely used in epithelial cancer as second-line or subsequent treatments (34). In terms of SC, anti-angiogenic targeted therapy has shown favorable efficacy in PSC. Specifically, anti-angiogenic monotherapy with apatinib has shown favorable efficacy in a patient with PSC with no notable adverse side effects (34). A retrospective study included 16 patients with PSC who received chemotherapy combined with bevacizumab or chemotherapy alone. Patients receiving combination therapy achieved a median PFS of 4.2 months and an OS of 11.2 months, outperforming chemotherapy-alone (median PFS, 1.2 months; OS, 7.9 months) (35). Anlotinib is a multi-target tyrosine kinase inhibitor of tumor neovascularization, which has shown favorable efficacy in SC as well as in epithelial cancer. In one case report, a patient with PSC achieved complete response for >20 months after treatment with anlotinib combined with tislelizumab as a second-line treatment (36). Furthermore, a patient with recurrent SC of the head and neck achieved long term PFS (>2 years) after treatment with sintilimab combined with anlotinib (33).

The tumor microenvironment (TME) functions as a key determinant in modulating immune responses and can impact the efficacy of ICIs (37). The anti-tumor immune response begins with the release of tumor cell antigen, followed by antigen processing and presentation by antigen-presenting cells (APCs), subsequent priming and mobilization of adaptive immunity, translocation of effector lymphocytes to the tumor site, infiltration of these immune effectors in the TME, recognition and finally destruction of cancer cells by effector cytotoxic T lymphocytes (mainly $CD8^+$ T lymphocytes) (37). The vascular landscape within the TME, along with diverse immune cells and cytokines, exerts distinct modulatory effects on the antitumor immune response. By modulating these elements, the efficacy of immunotherapy can be influenced.

The patient described in the present case report achieved PR following two cycles of durvalumab combined with anlotinib, despite having only achieving SD with prior treatment with chemoradiotherapy and anlotinib. This sequential efficacy pattern raises important questions regarding the baseline immune status of the tumor and the potential role of anlotinib and chemoradiotherapy in remodeling the TME.

The elevated CPS of 80 in the present case indicates a potentially immune-hot TME. The high PD-L1 expression likely reflects an adaptive reaction to lymphocyte-derived cytokines, specifically IFN-γ released by cytotoxic $CD8^+$ cells. Paradoxically, the same immune surveillance that detects malignancy simultaneously equips the tumor with inhibitory defenses, creating a primed yet suppressed microenvironment where ICIs can unleash pre-existing antitumor potential (38). However, while frequently associated with elevated PD-L1 levels, this is not a universal rule, and necessitates further immunohistochemical validation.

We hypothesize that the prior chemoradiotherapy and anlotinib treatment may have functioned as a 'priming' phase that further amplified this pre-existing immune-hot state. As documented in the literature, chemoradiotherapy triggers immunogenic cell death mechanisms, leading to the liberation of tumor-specific antigens, alongside various damage-associated molecular patterns, which include heat shock proteins (HSP70/90), high-mobility group box 1 and calreticulin (39). These molecules can promote the maturation of APCs and potentiate $CD8^+$ T cell functions (36). Furthermore, platinum agents can reshape immune landscapes by selectively eliminating myeloid-derived suppressor cells and regulatory T cells, thus relieving the inhibition of effector T cells (39). Simultaneously, radiotherapy promotes type I interferon responses and enhances dendritic cell (DC) cross-presentation, thus strengthening antitumor immunity (40).

Anlotinib appears to exert synergistic effects when combined with immunotherapy during cancer treatment. Mouse models of different types of cancer show that anlotinib can enhance ICIs efficacy through remodeling of tumor vasculature (41,42). Vascular normalization can reverse the immunosuppressive state of tumors and allow $CD8^+$ T cells to infiltrate tumors (41,42). Anlotinib can also downregulate PD-1, mucin domain-containing protein 3, immune checkpoint T-cell immunoglobulin and lymphocyte-activation gene 3, as well as increase the secretion of IFN-γ and TNF-α from T cells, thus preserving $CD8^+$ T-cell cytotoxicity (41,42). Furthermore, anlotinib can increase the levels of M1-polarized macrophages and reduce M2 subtypes, enhance major histocompatibility complex-I/II expression on tumor cells and promote DC maturation and antigen presentation, thus shifting the TME from an immunosuppressive to an immunostimulatory state and sustain immune memory (42). Accordingly, we hypothesize that prior exposure to anlotinib could potentiate tumor responsiveness to immunotherapeutic interventions.

However, it must be acknowledged that without serial biopsies during treatment, a definitive distinction cannot be made between: i) A pre-existing immune-hot TME that was activated by ICIs; ii) an anlotinib-mediated conversion from an intermediate state to an immune-hot state; and iii) the induction of an immune-hot TME state by chemoradiotherapy. Nevertheless, due to evidence from prior studies, the high baseline CPS and the pattern of treatment response, it may be hypothesized that the patient exhibited a baseline immune-hot state that was subsequently amplified by chemoradiotherapy and in particular anlotinib.

Although immunotherapy demonstrated promising efficacy, it was terminated due to severe adverse events in the present case. Maintenance therapy with anlotinib was continued and the tumor remains stable to date. To the best of our knowledge, this case study is among the first case reports to investigate the efficacy of ICIs and anti-angiogenic targeted therapy in mediastinal SC. The present case demonstrates the efficacy of immunotherapy combined with anlotinib on mediastinal SC with high expression of PD-L1.

There are several possible mechanisms underlying the sustained efficacy of anlotinib after ICI discontinuation in the present case. Firstly, treatment-free survival after discontinuation of ICIs has been observed in numerous patients with objective response, especially in those who stop use of ICIs due to immune-related adverse events (43). ICIs achieve clinical efficacy by activation and expansion of T and B lymphocytes, including memory T cells. Memory T cells can exhibit notable longevity and can exert an antitumor response following recognition of tumor-associated antigens; consequently, ICIs may maintain efficacy following discontinuation (43). Furthermore, immunotherapy combined with anlotinib appears to exert synergistic effects in cancer treatment as previously described (41,42). Through pleiotropic mechanisms, anlotinib reverses TME immunosuppression while promoting antigen-specific memory T cell persistence (41,42). Consequently, Even ICIs is stopped, anlotinib can sustain the efficacy of it.

In conclusion, the present case report demonstrates the potential of ICIs combined with anti-angiogenic targeted therapy in treating PD-L1-positive mediastinal SC, despite the life-threatening adverse reactions caused by ICIs. However, more prospective studies are required to confirm its efficacy and safety.

Acknowledgements

Not applicable.

Funding

No funding was received.

Availability of data and materials

The data generated in the present study may be requested from the corresponding author.

Authors' contributions

SW and DW were responsible for data collection, literature review and writing the manuscript. SW and QF were responsible for collecting images and data. SW, YD made substantial contributions to conception and design, revising the manuscript critically for important intellectual content. All authors have read and approved the manuscript. SW and YD confirm the authenticity of all the raw data.

Ethics approval and consent to participate

The study was approved by the Medical Ethics Committee of The First People's Hospital of Xiaoshan District (approval no. XYYLS Zi 2025No.01).

Patient consent for publication

Written informed consent was obtained from the patient's legal representative for the publication of this case report, including the publication of all images, clinical data and other data included in the manuscript.

Competing interests

The authors declare that they have no competing interests.

References

1. Xu Z, Wang L, Tu L, Liu Y, Xie X, Tang X and Luo F: Epidemiology of and prognostic factors for patients with sarcomatoid carcinoma: A large population-based study. Am J Cancer Res 10: 3801-3814, 2020.
2. Malla M, Wang JF, Trepeta R, Feng A and Wang J: Sarcomatoid carcinoma of the urinary bladder. Clin Genitourin Cancer 14: 366-372, 2016.
3. Li X, Wu D, Liu H and Chen J: Pulmonary sarcomatoid carcinoma: Progress, treatment and expectations. Ther Adv Med Oncol 12: 1758835920950207, 2020.
4. Liao SH, Su TH, Jeng YM, Liang PC, Chen DS, Chen CH and Kao JH: Clinical manifestations and outcomes of patients with sarcomatoid hepatocellular carcinoma. Hepatology 69: 209-221, 2019.
5. Piao ZH, Chen JP, Chen HR and Zhou XC: Malignant transformation of metaplastic thymoma into high-grade sarcomatoid carcinoma: A case report. Int J Surg Pathol 30: 564-568, 2022.
6. Moritani S, Ichihara S, Mukai K, Seki Y, Inoue S, Yasuda A, Hakiri S, Yatabe Y and Eimoto T: Sarcomatoid carcinoma of the thymus arising in metaplastic thymoma. Histopathology 52: 409-411, 2008.
7. Wick MR, Scheithauer BW, Weiland LH and Bernatz PE: Primary thymic carcinomas. Am J Surg Pathol 6: 613-630, 1982.
8. Shimizu J, Kamesui T, Moriya M, Murata S, Nakanishi I, Sasaki M and Minato H: Four cases of invasive anterior mediastinal tumors definitively diagnosed by the chamberlain procedure. Ann Thorac Cardiovasc Surg 20: 434-440, 2014.
9. Chalabreysse L, Etienne-Mastroianni B, Adeleine P, Cordier JF, Greenland T and Thivolet-Bejui F: Thymic carcinoma: A clinicopathological and immunohistological study of 19 cases. Histopathology 44: 367-374, 2004.
10. Wang Y, Yang L, Wang J, Gui L, Li W, Liu Z, Ma X, Yang Y, Wang L and Bi N: Case report: First case of consolidation immunotherapy after definitive chemoradiotherapy in mediastinal lymph node metastatic sarcomatoid carcinoma. Front Oncol 11: 788856, 2022.
11. Karakuchi N, Yanagawa S, Kushitani K, Kodama S, Takeshima Y and Sumimoto K: Primary small intestinal sarcomatoid carcinoma: Report of a rare case and literature review. Case Rep Oncol 14: 538-544, 2021.
12. Wenig BM: Squamous cell carcinoma of the upper aerodigestive tract: Dysplasia and select variants. Mod Pathol 30 (Suppl 1): S112-S118, 2017.
13. Marx A, Chan JKC, Chalabreysse L, Dacic S, Detterbeck F, French CA, Hornick JL, Inagaki H, Jain D, *et al*: The 2021 WHO Classification of Tumors of the Thymus and Mediastinum: What is New in Thymic, Epithelial, Germ Cell, and Mesenchymal Tumors? J Thorax Oncol 17: 200-213, 2022.
14. Weissferdt A: Spindle cell thymoma and its histological mimickers. Mediastinum 7: 32, 2023.
15. Baldovini C, Rossi G and Ciarrocchi A: Approaches to tumor classification in pulmonary sarcomatoid carcinoma. Lung Cancer (Auckl) 10: 131-149, 2019.
16. Ding K, Peng Z and Xu Y: Role of immunotherapy in pulmonary sarcomatoid carcinoma: Review of current approaches and related biomarkers. Ther Adv Med Oncol 16: 17588359241249041, 2024.
17. Huang Y, Guo J, Li S, Liu J, Xu J, Ye W, Zhang L, Dong Z, Wu W and Wu C: The correlation between histologic, immunophenotypic, and molecular characteristics of pulmonary sarcomatoid carcinoma reveals that sarcomatoid change is potentially derived from epithelial carcinoma cells undergoing epithelial-mesenchymal transition. Appl Immunohistochem Mol Morphol 31: 17-25, 2023.
18. Zeng Q, Li J, Sun N, Xue Q, Gao Y, Zhao J, Mao Y, Mu J, Wang D, Gao S and He J: Preoperative systemic immune-inflammation index predicts survival and recurrence in patients with resected primary pulmonary sarcomatoid carcinoma. Transl Lung Cancer Res 10: 18-31, 2021.
19. Ma S, Li C, Ma Y, Wang X, Zhang D and Lu Z: A retrospective study on the clinical and pathological features of hepatic sarcomatoid carcinoma: Fourteen cases of a rare tumor. Medicine (Baltimore) 101: e30005, 2022.

20. Vieira T, Girard N, Ung M, Monnet I, Cazes A, Bonnette P, Duruisseaux M, Mazieres J, Antoine M, Cadranel J and Wislez M: Efficacy of first-line chemotherapy in patients with advanced lung sarcomatoid carcinoma. J Thorac Oncol 8: 1574-1577, 2013.
21. Lara PN Jr, Redman MW, Kelly K, Edelman MJ, Williamson SK, Crowley JJ and Gandara DR; Southwest Oncology Group: Disease control rate at 8 weeks predicts clinical benefit in advanced non-small-cell lung cancer: Results from southwest oncology group randomized trials. J Clin Oncol 26: 463-467, 2008.
22. Zhu Z, Liu X, Li W, Wen Z, Ji X, Zhou R, Tuo X, Chen Y, Gong X, Liu G, *et al*: A rare multiple primary sarcomatoid carcinoma (SCA) of small intestine harboring driver gene mutations: A case report and a literature review. Transl Cancer Res 10: 1150-1161, 2021.
23. Sun L, Dai J, Chen Y, Duan L, He W, Chen Q, Wang H, Zhu Y, Zhang H, Jiang G and Zhang P: Pulmonary sarcomatoid carcinoma: Experience from SEER database and Shanghai pulmonary hospital. Ann Thorac Surg 110: 406-413, 2020.
24. Rahouma M, Kamel M, Narula N, Nasar A, Harrison S, Lee B, Stiles B, Altorki NK and Port JL: Pulmonary sarcomatoid carcinoma: An analysis of a rare cancer from the surveillance, epidemiology, and end results database. Eur J Cardiothorac Surg 53: 828-834, 2018.
25. Reck M, Rodríguez-Abreu D, Robinson AG, Hui R, Csőszi T, Fülöp A, Gottfried M, Peled N, Tafreshi A, Cuffe S, *et al*: Pembrolizumab versus chemotherapy for PD-L1-positive non-small-cell lung cancer. N Engl J Med 375: 1823-1833, 2016.
26. Mok TSK, Wu YL, Kudaba I, Kowalski DM, Cho BC, Turna HZ, Castro G Jr, Srimuninnimit V, Laktionov KK, Bondarenko I, *et al*: Pembrolizumab versus chemotherapy for previously untreated, PD-L1-expressing, locally advanced or metastatic non-small-cell lung cancer (KEYNOTE-042): A randomised, open-label, controlled, phase 3 trial. Lancet 393: 1819-1830, 2019.
27. Sezer A, Kilickap S, Gümüş M, Bondarenko I, Özgüroğlu M, Gogishvili M, Turk HM, Cicin I, Bentsion D, Gladkov O, *et al*: Cemiplimab monotherapy for first-line treatment of advanced non-small-cell lung cancer with PD-L1 of at least 50%: A multicentre, open-label, global, phase 3, randomised, controlled trial. Lancet 397: 592-604, 2021.
28. Kim S, Kim MY, Koh J, Go H, Lee DS, Jeon YK and Chung DH: Programmed death-1 ligand 1 and 2 are highly expressed in pleomorphic carcinomas of the lung: Comparison of sarcomatous and carcinomatous areas. Eur J Cancer 51: 2698-2707, 2015.
29. Silvestris N, Argentiero A, Brunetti O, Sonnessa M, Colonna F, Delcuratolo S, Luchini C, Scarpa A, Lonardi S, Nappo F, *et al*: PD-L1 and Notch as novel biomarkers in pancreatic sarcomatoid carcinoma: a pilot study. Expert Opin Ther Targets 25: 1007-1016, 2021.
30. Roesel C, Kambartel K, Kopeika U, Berzins A, Voshaar T and Krbek T: Lazarus-type tumour response to therapy with nivolumab for sarcomatoid carcinomas of the lung. Curr Oncol 26: e270-e273, 2019.
31. Qian X, Wang Y, Liu F, Yuan Y, Fang C, Zhang X, Yuan S, Chen R, Yu B, Wang T, *et al*: The efficacy and safety analysis of first-line immune checkpoint inhibitors in pulmonary sarcomatoid carcinoma. Front Immunol 13: 956982, 2022.
32. Wei JW, Hao Y, Xiang J, Pu XX, Wang LP, Jiang ZS, Wu JX, Wang Q, Xu CW, Wang WX and Song ZB: The prognostic impact of immune checkpoint inhibitors for the treatment of pulmonary sarcomatoid carcinoma: A multicenter retrospective study. Neoplasma 69: 1437-1444, 2022.
33. Wang L, Huang Y and Sun X: Sintilimab combined with anlotinib as first-line treatment for advanced sarcomatoid carcinoma of head and neck: A case report and literature review. Front Oncol 14: 1362160, 2024.
34. Li X, He Y, Zhu J, Pang H, Lin Y and Zheng J: Apatinib-based targeted therapy against pulmonary sarcomatoid carcinoma: A case report and literature review. Oncotarget 9: 33734-33738, 2018.
35. Oizumi S, Takamura K, Harada T, Tachihara M, Morikawa N, Honda R, Watanabe S, Asao T, Kunisaki M, Fukuhara T, *et al*: Phase II study of carboplatin-paclitaxel alone or with bevacizumab in advanced sarcomatoid carcinoma of the lung: HOT1201/NEJ024. Int J Clin Oncol 27: 676-683, 2022.
36. Li YF, Zhao XF, Tian Y, Xiao XY, Yan CY and Shen H: Case report: Pulmonary sarcomatoid carcinoma complicating TP53 mutation treated successfully with Tislelizumab combined with Anlotinib-a case report. Front Genet 13: 949989, 2022.
37. Wang P, Xu S, Guo Q and Zhao Y: Discovery of PAK2 as a key regulator of cancer stem cell in head and neck squamous cell carcinoma using multi-omic techniques. Stem Cells Int 2025: 1325262, 2025.
38. Dosset M, Vargas TR, Lagrange A, Boidot R, Végran F, Roussey A, Chalmin F, Dondaine L, Paul C, Lauret Marie-Joseph E, *et al*: PD-1/PD-L1 pathway: An adaptive immune resistance mechanism to immunogenic chemotherapy in colorectal cancer. Oncoimmunology 7: e1433981, 2018.
39. Wang Y, Lu K, Xu Y, Xu S, Chu H and Fang X: Antibody-drug conjugates as immuno-oncology agents in colorectal cancer: Targets, payloads, and therapeutic synergies. Front Immunol 16: 1678907, 2025.
40. Saxena A: Combining radiation therapy with immune checkpoint blockade for the treatment of small cell lung cancer. Semin Cancer Biol 90: 45-56, 2023.
41. Shan Y, Zhong C, Ni Q, Zhang M, Wang G and Zhou F: Anlotinib enhanced penpulimab efficacy through remodeling of tumor vascular architecture and immune microenvironment in hPD-L1/hPD-1 humanized mouse model. J Clin Oncol 39: (15Suppl): S2581, 2021.
42. Su Y, Luo B, Lu Y, Wang D, Yan J, Zheng J, Xiao J, Wang Y, Xue Z, Yin J, *et al*: Anlotinib induces a T cell-inflamed tumor microenvironment by facilitating vessel normalization and enhances the efficacy of PD-1 checkpoint blockade in neuroblastoma. Clin Cancer Res 28: 793-809, 2022.
43. Vacher L, Bernadach M, Molnar I, Passildas-Jahanmohan J and Dubray-Longeras P: The efficacy of immune checkpoint inhibitors following discontinuation for long-term response or toxicity in advanced or metastatic non-small-cell lung cancers: A retrospective study. Health Sci Rep 7: e1825, 2024.